Crossover and coexistence of superconductivity and antiferromagnetism in the filled-skutterudite system $Pr_{1-x}Eu_xPt_4Ge_{12}$

I. Jeon,[1,2] S. Ran,[2,3] A. J. Breindel,[2,3] P.-C. Ho,[4] R. B. Adhikari,[5] C. C. Almasan,[5] B. Luong,[3] and M. B. Maple[1,2,3,*]

[1]*Materials Science and Engineering Program, University of California, San Diego, La Jolla, California 92093, USA*
[2]*Center for Advanced Nanoscience, University of California, San Diego, La Jolla, California 92093, USA*
[3]*Department of Physics, University of California, San Diego, La Jolla, California 92093, USA*
[4]*Department of Physics, California State University Fresno, Fresno, California 93740, USA*
[5]*Department of Physics, Kent State University, Kent, Ohio, 44242, USA*

(Dated: January 9, 2017)

The superconducting and normal-state properties of the filled-skutterudite system $Pr_{1-x}Eu_xPt_4Ge_{12}$ were studied. Polycrystalline samples were investigated via x-ray diffraction, electrical resistivity, magnetic susceptibility, and specific heat measurements. Upon Eu substitution, we observed a crossover from superconducting to antiferromagnetic states with a region where both states coexist. In the superconducting region, the specific heat data exhibit a change of temperature dependence, suggesting an evolution from a nodal to a nodeless superconducting energy gap or a suppression of multiband superconductivity. This change is relatively slower than those reported for different substituent ions, suggesting paramagnetic impurities have a weaker pair breaking effect on unconventional superconductivity in $PrPt_4Ge_{12}$. In the normal state, an evolution from Fermi-liquid to non-Fermi-liquid behavior was observed, accompanied by the coexistence of superconductivity and antiferromagnetism, suggesting the underlying electronic structure is primarily responsible for the complex physical phenomena found in this system.

PACS numbers: 71.10.Ay, 74.25.Dw, 74.62.Bf, 75.40.-s

I. INTRODUCTION

A new class of filled-skutterudite compounds with the chemical formula MPt_4Ge_{12} (M = alkali metal, alkaline earth, lanthanide, or actinide) has recently been reported [1–7]. These new Pt-Ge based skutterudite systems exhibit various strongly correlated electron phenomena. The compound $PrPt_4Ge_{12}$ is especially interesting since it is an unconventional superconductor that has properties similar to those of $PrOs_4Sb_{12}$: point nodes in the superconducting energy gap indicated by transverse muon spin relaxation (μSR) and specific heat measurements, evidence for time-reversal symmetry breaking (TRSB) from zero-field μSR measurements [5,8], and multiband unconventional superconductivity (SC) suggested from previous reports [9–11]. Several chemical substitution studies based on specific heat measurements reveal a suppression of superconductivity in $PrPt_4Ge_{12}$, accompanied by a crossover from a nodal to a nodeless superconducting energy gap or the suppression of multiple superconducting energy bands with increasing substituent composition [12–14].

Unconventional SC seems to be correlated with magnetism. The interplay between these two phenomena often leads to rich and intriguing physics with complex temperature T versus substituent composition or applied pressure phase diagrams, including pseudogaps, structural phase transitions, non-Fermi-liquid (NFL) behavior, or quantum criticality. In many Fe-pnictide and cuprate compounds, the interplay between unconventional SC and antiferromagnetic (AFM) order is manifested in generic phase diagrams, in which the unconventional SC appears to emerge in a dome shaped region near the composition or pressure where the antiferromagnetic order has been suppressed towards 0 K [15,16]. The filled-skutterudite system $Pr_{1-x}Nd_xOs_4Sb_{12}$ shows the effect of magnetic moments on the normal and SC states of $PrOs_4Sb_{12}$, suggesting superconductivity and magnetism coexist within the superconducting state [17,18]. However, such an interplay between magnetism and unconventional SC in $PrPt_4Ge_{12}$ has not yet been reported, to the best of our knowledge.

In the end member compound $EuPt_4Ge_{12}$, the Eu ion is divalent and the electronic configuration is the same as Gd^{3+} ion, $J = S = 7/2$. The compound $EuPt_4Ge_{12}$ orders antiferromagnetically with a Néel temperature, $T_N \sim 1.7$ K with an effective magnetic moment, $\mu_{eff} \sim 7.4$ μ_B and a Curie-Weiss temperature, $\Theta_{CW} \sim -11$ K [19]. The value of T_N for $EuPt_4Ge_{12}$ is fairly low compared to other Eu-based filled-skutterudite compounds with the Eu^{2+} electronic configuration. For example, the compounds $EuFe_4X_{12}$ (X = Sb, As) are ferromagnetic with Curie temperatures, $T_c \sim 88$ K and ~ 152 K, respectively, where the enhanced T_c has been attributed to the existence of a small magnetic moment (~ 0.21 μ_B for the Fe-Sb cage) on the Fe ion [20,21]. The low T_N value for $EuPt_4Ge_{12}$ is possibly due to absence of a magnetic moment on Pt in the Pt-Ge cage, leading to a decrease of the Ruderman-Kittel-Kasuya-Yosida (RKKY) interaction between the Eu^{2+} localized magnetic moment and the conduction electrons spins [19,22]. This is seen in previous reports for the compounds $EuRu_4X_{12}$ with non-magnetic Ru-X cages (ferromagnetic transition temperature, $T_m \sim 3.3$ K for X = Sb and no magnetic anomaly down to 2 K for X = As) [20,21,23]. In addition, $EuPt_4Ge_{12}$ has a large Sommerfeld coefficient, $\gamma \sim$

220 mJ/mol K, which has been attributed to Eu^{2+} spin fluctuations [19,24].

In this paper, we report a study of the $Pr_{1-x}Eu_xPt_4Ge_{12}$ system. The evolution of superconducting and magnetic properties with increasing Eu concentration, x, was studied by means of x-ray diffraction, electrical resistivity, magnetic susceptibility, and specific heat measurements. We observed a crossover from SC to AFM and a suppression of SC with negative curvature as a function of x, and a Eu concentration range within which the two phases coexist. Our results from specific heat measurements are similar to those of previous studies ($Pr_{1-x}Ce_xPt_4Ge_{12}$ and $PrPt_4Ge_{12-x}Sb_x$), suggesting a possible crossover from a nodal to a nodeless superconducting energy gap or from multiple energy gaps to a single BCS-type superconducting energy gap [9–14]; however, the crossover in the present case is much slower. In the normal state, we observed a crossover from Fermi-liquid (FL) to non-Fermi-liquid (NFL) behavior in the Eu rich region, suggesting the intrinsic electronic structure is correlated to SC, AFM, and other possible complex physical phenomena in this system.

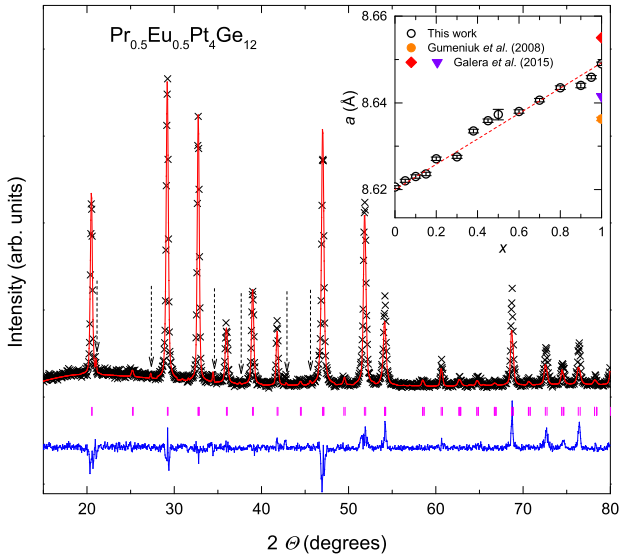

FIG. 1: (Color online) X-ray diffraction pattern for $Pr_{0.5}Eu_{0.5}Pt_4Ge_{12}$. The black crosses represent the experimental data and the red line represents the fit from the Rietveld refinement of the data. The magenta vertical marks indicate the position of expected Bragg reflections and the blue line at the bottom is the difference between observed and calculated intensities. The dashed arrows indicate Bragg reflections associated with a Ge or $PtGe_2$ impurity phase. The inset shows a plot of the lattice parameter a versus nominal Eu concentration x. The red dashed line is a guide to the eye.

II. EXPERIMENTAL DETAILS

Polycrystalline samples of $Pr_{1-x}Eu_xPt_4Ge_{12}$ were synthesized by arc-melting on a water-cooled copper hearth under an Ar atmosphere with a Zr getter and then annealed. The starting materials were Pr ingots (Alfa Aesar 99.9%), Eu ingots (Alfa Aesar 99.9%), Pt sponge (Engelhard 99.95%), and Ge pieces (Alfa Aesar 99.9999+%). The detailed procedures used to prepare the samples are reported elsewhere [13]. The crystal structure was determined by x-ray powder diffraction (XRD) using a Bruker D8 Discover x-ray diffractometer with Cu-K_α radiation, and XRD patterns were analyzed via Rietveld refinement using the GSAS+EXPGUI software package [25,26]. The electrical resistivity was measured from 1.1 K to 300 K using a standard four-wire method with a Linear Research LR700 AC resistance bridge in a home-built probe in a liquid ^{4}He Dewar, and down to $\sim$ 100 mK (data below 0.35 K were rejected due to noise) using a commercial ^{3}He-^{4}He dilution refrigerator. Magnetic susceptibility measurements were made between 2 K and 300 K in magnetic fields up to 7 T using a Quantum Design Magnetic Property Measurement System (MPMS). Specific heat measurements were performed at temperatures down to 1.8 K with a Quantum Design Physical Property Measurement System (PPMS) DynaCool and down to 0.5 K with the ^{3}He option for the PPMS DynaCool.

III. RESULTS

A. X-ray diffraction

Figure 1 shows results from XRD data for the $Pr_{1-x}Eu_xPt_4Ge_{12}$ ($0 \leq x \leq 1$) system. All of the XRD patterns are well indexed with the cubic filled-skutterudite crystal structure with space group $Im\bar{3}$. Figure 1 displays a representative XRD pattern of the $Pr_{0.5}Eu_{0.5}Pt_4Ge_{12}$ compound and the best fit from the Rietveld refinement. The dashed arrows indicate the contents of small impurity phases of Ge and/or $PtGe_2$ (at most up to $\sim$ 5% by molar mass ratio), as is commonly observed in the Pt-Ge based skutterudites [3,4,7,9,11,13, 27,28]. Since Eu ions are divalent in the end member compound $EuPt_4Ge_{12}$ [19,24], and the atomic radius of Eu^{2+} ions is larger than that of the Pr^{3+} ions, the lattice parameter a exhibits a linear increase throughout the entire range of x, as shown in the inset of Fig. 1; however, there are discrepancies in the a values for $EuPt_4Ge_{12}$ between previous reports and our study, which is possibly due to a known sample dependence in the Pt-Ge based filled skutterudites; reported values of a for $EuPt_4Ge_{12}$ differ by roughly 0.5% [3,28].

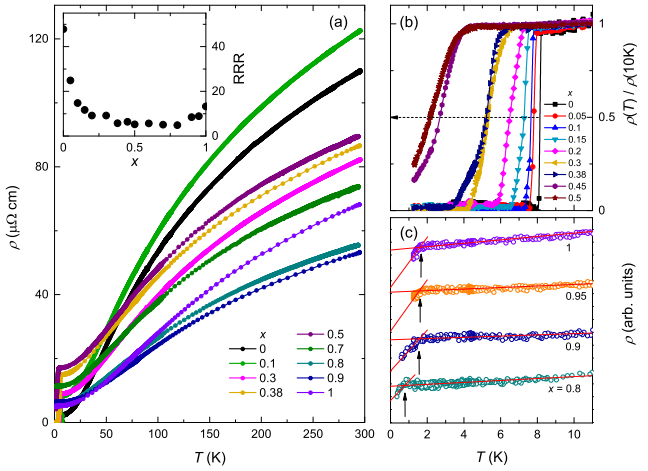

FIG. 2: (Color online) (a) Electrical resistivity data ρ versus T for selected $Pr_{1-x}Eu_xPt_4Ge_{12}$ samples. Displayed in the inset is a plot of the residual resistivity ratio RRR versus x for $Pr_{1-x}Eu_xPt_4Ge_{12}$. The RRR shows a parabolic shape with the minimum at $x = 0.5$. (b) $\rho(T)$, normalized to its value at 10 K, versus x for superconducting $PrPt_4Ge_{12-x}Sb_x$ samples. The superconducting transition temperature, T_c, decreases with increasing x. The dashed arrow is a guide to the eye. (c) $\rho(T)$ versus x with offsets for Eu rich compounds exhibiting kinks associated with an antiferromagnetic transition, indicated by solid arrows. The Néel temperature, T_N, decreases slowly from $x = 1$ to 0.8.

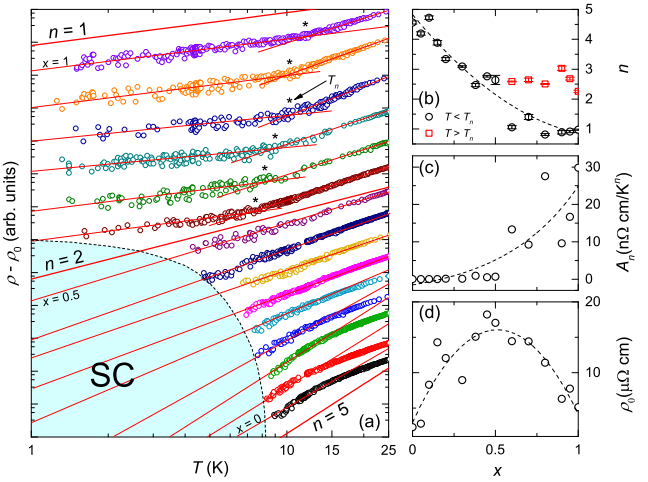

FIG. 3: (Color online) (a) A double logarithmic plot of $\rho - \rho_0$ versus T for $Pr_{1-x}Eu_xPt_4Ge_{12}$ with vertical translations for visual clarity. Linear fits of Eq. 1 were made to data up to $T \sim 15$ K, indicated by the red solid lines. The gradual change of n from ~ 5 at $x = 0$ to ~ 1 at $x = 1$ was observed. The thicker solid lines are for reference, with different n values ($n = 1$, 2, and 5, respectively). The black asterisks point out the temperatures where the value of n changes for Eu rich compounds. The light blue filled area denotes the SC region. The corresponding fitting parameters n and A, and residual resistivity ρ_0, versus x are shown in (b), (c), and (d), respectively.

B. Electrical Resistivity

The results of electrical resistivity, $\rho(T)$, measurements are shown in Fig. 2. All samples exhibit metallic behavior in their normal states, as seen in Fig. 2(a); we show some representative concentrations for visual clarity. The residual resistivity ratio, RRR (ρ_{300}/ρ_0), versus x is shown in the inset of Fig. 2(a), where ρ_{300} is the room temperature resistivity and ρ_0 is the resistivity value right above the SC/AFM transitions. The RRR(x) exhibits a parabolic shape with the minimum around $x = 0.5$, consistent with the expected minimum for simple alloys. Figure 2(b) displays $\rho(T)$ normalized to its value at 10 K versus x. The T_c value was defined as the temperature where the value of $\rho(T)/\rho_{10}$ drops to 0.5, and the width of the transition was determined by the temperatures where $\rho(T)/\rho_{10}$ is 0.9 and 0.1. A monotonic decrease of T_c is observed to $x = 0.5$, with slightly broadened transitions for $x > 0.3$. We also performed $\rho(T)$ measurements down to 0.35 K on the selected samples with $x = 0.6$, 0.8, and 0.9; however, there was no sign of SC. In Fig. 2(c), $\rho(T)$ data for Eu rich compounds, shown with vertical translations for visual clarity, exhibit kinks associated with AFM transitions [19]. The Néel temperature, T_N, decreases from ~ 1.7 K for $x = 1$ to ~ 0.8 K for $x = 0.8$; we did not observe any clear feature associated with the AFM transitions for samples with $x < 0.8$, down to 0.35 K.

Fig. 3(a) shows a log-log plot of $\rho - \rho_0$ versus T with vertical translations for visual clarity. The red solid lines represent least squares fits to the data with the formula:

$$\log(\rho(T) - \rho_0) = \log(A_n) + n\log(T), \qquad (1)$$

in the temperature range from just above T_c or T_N to ~ 15 K. Interestingly, a gradual change of n values was observed throughout the entire substitution range from $n \sim 5$ at $x = 0$ to $n \sim 1$ at $x = 1$. For Pr rich samples, they are consistent with the Bloch-Grüneisen behavior, since they have rather large n values from ~ 4 to ~ 5 as seen in Fig. 2 (a). The negative curvature of $\rho(T)$ at elevated temperatures is indicative of a narrow feature in the electronic density of states at the Fermi level [29]. For $EuPt_4Ge_{12}$, it has been reported that evidence of a FL ground state, a T^2 dependence of $\rho(T)$, is not recovered even under applied magnetic field at 12 T [19], suggesting that system may show a crossover from a FL to a NFL ground state. For $x > 0.5$, we observe kinks in Fig. 3 (a), where the slopes, n, change. As shown in Fig. 3 (b), the value of n decreases from ~ 5 to 1, suggesting a type of crossover from FL to NFL behavior with decreasing temperature; this result may indicate that magnetic fluctuations associated with Eu ions in the $EuPt_4Ge_{12}$ [19] become even weaker with increasing Pr substitution. The corresponding fitting parameters A_n and ρ_0 versus x are shown in Fig. 3 (c) and (d), respectively. The coefficient, A_n, increases monotonically while the residual resistivity, ρ_0, has a parabolic shape with a maximum at $x \sim$

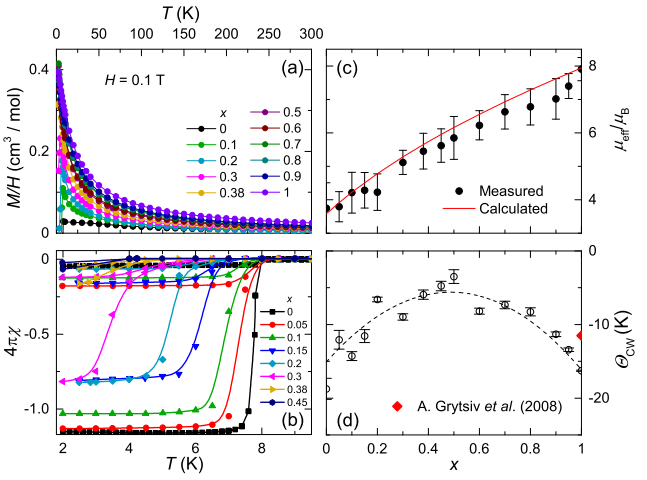

FIG. 4: (Color online) (a) A plot of magnetization divided by applied magnetic field, M/H, versus temperature T, measured in an applied magnetic field $H = 0.1$ T for selected samples of $Pr_{1-x}Eu_xPt_4Ge_{12}$ for visual clarity. (b) The Meissner and diamagnetic shielding fractions $4\pi\chi$ versus T for superconducting samples. The diamagnetic shielding fractions are close to 1. The deviations from unity are probably due to uncertainties in estimating the demagnetization factor. (c) Effective magnetic moment, obtained from the fit, $(\mu_{\rm eff}/\mu_{\rm B})$ versus x; the value of $\mu_{\rm eff}(x)/\mu_{\rm B}$ increases from $\mu_{\rm eff} \sim 3.7\ \mu_{\rm B}$ at $x = 0$ to $\mu_{\rm eff} \sim 7.9\ \mu_{\rm B}$ at $x = 1$. The red line is determined from a calculation using Eq. 3. (d) Curie-Weiss temperature $\Theta_{\rm CW}$ versus x. As x is increased, $\Theta_{\rm CW}$ first increases to $x \sim 0.5$ and then decreases to $x = 1$. The dashed lines are guides to the eye.

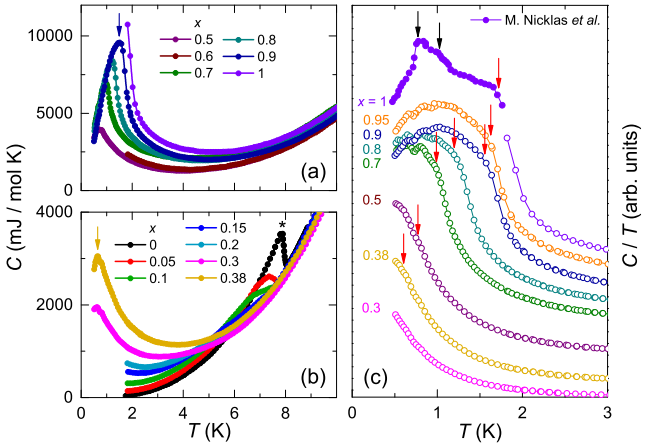

FIG. 5: (Color online) (a) and (b) Specific heat C versus temperature T for $Pr_{1-x}Eu_xPt_4Ge_{12}$. Arrows indicate features associated with AFM transitions and the black asterisk locates the SC anomaly. (c) C/T versus T data at low temperatures for Eu rich compounds. The Néel temperature, $T_{\rm N}$ are suppressed with increasing Pr content, as indicated by red arrows. The multiple magnetic transitions (black arrows) defined by M. Nicklas *et al.* [30] are shown as a reference.

0.5. The scatter in the values of $A_n(x)$ and $\rho_0(x)$ are probably due to uncertainties in the measurement of the geometrical factors of the resistivity samples.

C. Magnetic Susceptibility

Magnetization divided by applied magnetic field, M/H, versus T data are displayed in Fig. 4 (a). Measurements were made under an applied magnetic field of $H = 0.1$ T. The overall magnitude of M/H increases with increasing x, becoming more temperature dependent. Figure 4(b) shows superconducting transitions for $0 \leq x \leq 0.45$ in an applied magnetic field $H = 10$ Oe. We defined $T_{\rm c}$ as the temperature where zero-field-cooled (ZFC) and field-cooled (FC) data start to deviate from one another. The superconducting volume fractions were estimated from the ZFC $\chi(T)$ data by using the relation $4\pi\chi \times d$, where d is the molar density of the samples in units of mol/cm^3. The values of the volume fractions scatter around 1, which results from the uncertainties in determining demagnetization factors for this analysis. We fit the $M(T)/H$ data to a Curie-Weiss law in the temperature range from 50 to 300 K,

$$M/H = C_0/(T - \Theta_{\rm CW}), \qquad (2)$$

where C_0 is the Curie constant and $\Theta_{\rm CW}$ is the Curie-Weiss temperature. The average effective magnetic moment, $\mu_{\rm eff}$, of the Eu and Pr mixture is estimated using the relation $C_0 = \mu_{\rm eff}^2 N_{\rm A}/3k_{\rm B}$, where $N_{\rm A}$ is Avogadro's number and $k_{\rm B}$ is Boltzmann's constant. The best fit values are shown in Fig. 4 (c) and (d). Values of $\mu_{\rm eff}(x)$ increase from $\sim 3.7\ \mu_{\rm B}$ to $\sim 7.9\ \mu_{\rm B}$. The data are consistent with the calculated values, indicated by the red line in Fig. 4 (b), using the relation:

$$\mu_{\rm eff}(x) = \sqrt{(\mu_{\rm Pr^{3+}})^2(1-x) + (\mu_{\rm Eu^{2+}})^2(x)}, \qquad (3)$$

where the free ion values of $\mu_{\rm Pr^{3+}}$ and $\mu_{\rm Eu^{+2}}$ are 3.58 $\mu_{\rm B}$ and 7.94 $\mu_{\rm B}$, respectively. This result indicates the electronic structure of the Eu^{2+} ion is stable in our alloy system, as would be expected for Gd^{3+} substitution on $PrPt_4Ge_{12}$.

The dependence of the Curie-Weiss temperature, $\Theta_{\rm CW}$, on x has a parabolic shape with a maximum around $x \sim 0.5$, as shown in Fig. 4 (d). Note that for $PrPt_4Ge_{12}$, there is evidence of crystalline electric field (CEF) splitting of the Hund's rule ground state multiplet with a $\Gamma_4^{(1)}$ triplet as the first excited state [4], while there are no CEF effects in $EuPt_4Ge_{12}$ since Eu^{2+} is an S-state ion [19]. The systematic substitution of Eu for Pr could be a reason for the decrease in magnitude of the $\Theta_{\rm CW}$ up to $x \sim 0.5$, possibly due to the dilution of CEF effects. The increase in magnitude of $\Theta_{\rm CW}$ for $x \geq 0.5$ is probably due to the AFM order.

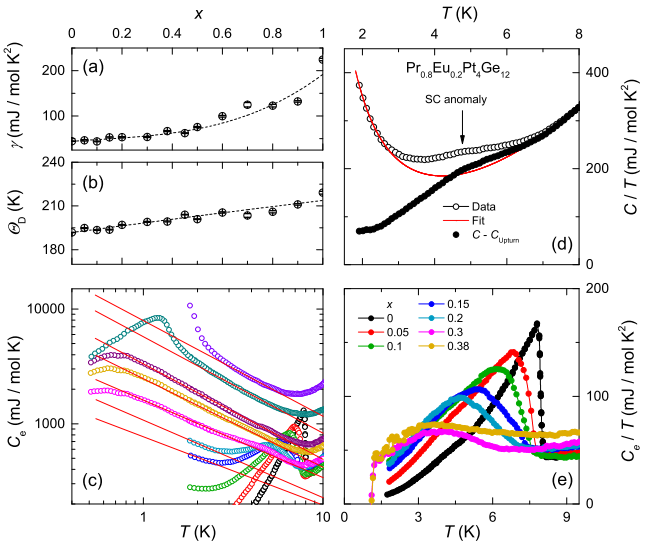

FIG. 6: (Color online) (a) and (b) Plots of the electronic specific heat cofficient, γ, and Debye temperature $\Theta_{\rm D}$, versus x. The values were obtained from linear fits of Eq. 4 to the data. The γ values first increase slowly to $x = 0.5$ then increase faster to $x = 1$ (see text), while the values of $\Theta_{\rm D}$ show a moderate increase with increasing x. Dashed lines are guides to the eye. (c) A systematic increase of the upturn in $C(T)$ at low temperature is displayed as a log-log plot of the electronic specific heat contribution, $C_{\rm e}$ versus T. Red lines are guides to the eye. (d) A procedure for subtraction of the upturn in $C(T)$ is displayed in a plot of C/T versus T for the superconducting $Pr_{0.8}Eu_{0.2}Pt_4Ge_{12}$ compound. Open circles are raw data, the red line is the fit, using Eq. 5, and the solid circles are the $C(T)$ data after subtraction of the upturn. (e) Plots of $C_{\rm e}$ versus T showing SC anomalies for $x < 0.45$ after subtraction of the low temperature upturn in $C(T)$ for each sample.

D. Specific Heat

Specific heat, C, versus T data are shown in Fig. 5(a) and (b) for selected samples for the sake of visual clarity. Anomalies associated with the onset of SC were observed in samples with $x < 0.45$. Since Néel temperatures, $T_{\rm N}$, are below 1.8 K in the resistivity data, we performed low-temperature specific heat measurements on samples with $x = 0.95$, 0.9, 0.8, 0.7, 0.5, 0.38, and 0.3, down to 0.5 K. In Fig. 5(c), the values of $T_{\rm N}$ (indicated by red arrows) are suppressed with increasing Pr content until $x \sim 0.38$. These results are consistent with those from the resistivity data. A previous study on $EuPt_4Ge_{12}$ by Nicklas *et al.* [24] reported that $EuPt_4Ge_{12}$ exhibits complex magnetic order at low temperature (indicated by black arrows in Fig. 5 (c)). It seems these additional transitions are suppressed with increasing Pr concentration for $x = 0.95$, 0.9, 0.8, and 0.7 at least; however, further investigations are needed, since the nature of this complex magnetic order has not yet been clarified.

The coefficients of the electronic and lattice contributions to the specific heat, γ and β, respectively, were determined using linear fits:

$$C(T)/T = \gamma + \beta T^2, \qquad (4)$$

in the range from the lowest non-ordered temperature to $\sim$ 250 K^2 (data not shown). In Fig. 6 (a), the γ values first increase from $\sim$ 45 mJ/mol K^2 at $x = 0$ to $\sim$ 76 mJ/mol K^2 at $x = 0.5$ in the SC region and then increase more rapidly up to $\sim$ 224 mJ/mol K^2 at $x = 1$ in the Eu rich region. Such different rates of increase in the γ values suggest that stronger electronic correlations or Eu^{2+} spin fluctuations, as reflected in the AFM nature of $EuPt_4Ge_{12}$ [19,22], are more clearly manifested in the Eu rich region. Even though the γ value for $x = 1$ is about half of $\gamma \sim 500$ mJ/mol K^2 for $PrOs_4Sb_{12}$ [31, 32], it is still a fairly large enhancement of γ; further research on $EuPt_4Ge_{12}$ would be of interest. The Debye temperature, $\Theta_{\rm D}$, was obtained using the relation: $\Theta_{\rm D} = [1944 \times (n_{\rm f.u.}/\beta)]^{1/3}$ K, where $n_{\rm f.u.} = 17$, the number of atoms in the formula unit. As seen in Fig. 6 (b), $\Theta_{\rm D}$ shows a small increase with increasing x.

Since the systematic upturns in specific heat at low temperature (see Fig. 5(b)) are simultaneously present with SC anomalies, our ability to determine the exact $T_{\rm c}$ values is compromised. The electronic contribution to the specific heat, $C_{\rm e}(T)$, was obtained by subtracting the phonon contribution, $C_{\rm ph}(T) = \beta T^3$, from the $C(T)$ data. A log-log plot of $C_{\rm e}$ versus T in Fig. 6 (c) shows the upturns in $C(T)$ have a power-law type divergence; the values of the slopes scatter around ~ -1. We, therefore, subtracted this upturn in $C(T)$ from the data, using the relation:

$$C(T) = \gamma T + \beta T^3 + pT^{-q}, \qquad (5)$$

where p and q are the fitting parameters. First, we fixed the γ and β values obtained from linear fits using Eq. 4 and performed least-squares fits of Eq. 5 to data, in order to determine p and q values and subtract only the upturn from the data. An example for $Pr_{0.8}Eu_{0.2}Pt_4Ge_{12}$ is displayed in Fig. 6 (d). The fitting parameter q scattered between $\sim$ 0.8 and $\sim$ 1.1, consistent with the observation in Fig. 6(c). The SC anomalies after subtraction of the upturns are shown as a plot of $C_{\rm e}/T$ versus T in Fig. 6 (e), showing a systematic decrease of $T_{\rm c}$, consistent with results obtained from resistivity and magnetization data. However, we did not observe clear features of SC for the $x = 0.45$ and 0.5 samples, possibly due to broad superconducting transitions and low $T_{\rm c}$ values.

Fig. 7 displays semilogarithmic plots of $C_e/\gamma T_{\rm c}$ versus $T_{\rm c}/T$ for $Pr_{1-x}Eu_xPt_4Ge_{12}$ up to $x = 0.3$. The fits to the data were performed in the range $1 \leq T_{\rm c}/T \leq T_{\rm c}/T_{\rm min}$, where $T_{\rm min}$ is the lowest temperature available in the data. The red lines in Fig. 7 (a,b,c) show that the compounds with $x \leq 0.1$ are best described by the power-law formula $b(T_{\rm c}/T)^{-m}$, where b and m are the fitting parameters, whose values are listed in Fig. 7. This power-law temperature-dependence suggests multiband superconductivity or nodes in the gap function in these

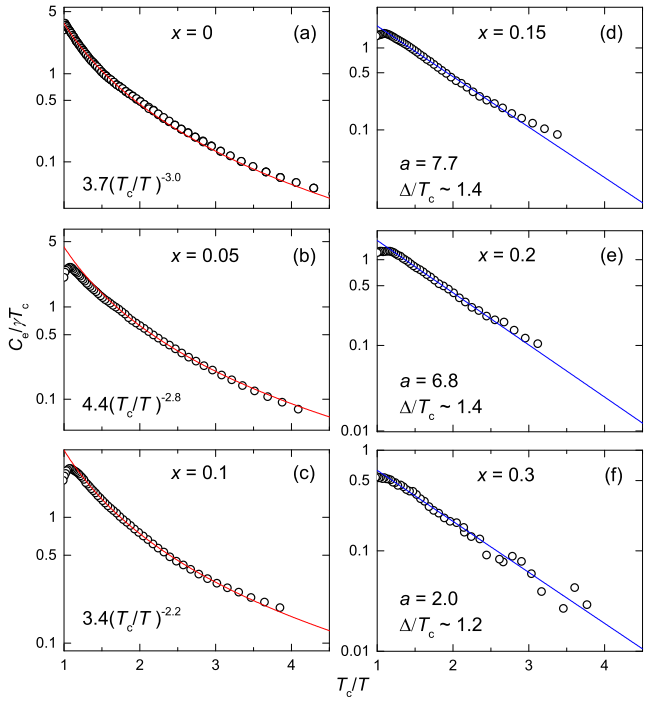

FIG. 7: (Color online) Semilogarithmic plots of the electronic contribution to specific heat, $C_e(T)/\gamma T_c$, below T_c, versus T_c/T for $Pr_{1-x}Eu_xPt_4Ge_{12}$ with $x = 0$, 0.5, 0.1, 0.15, 0.2, and 0.3. The red and blue lines represent the best fits to the data with (a, b, c) power-law behavior, $b(T_c/T)^{-m}$, and (d, e, f) exponential behavior, $ae^{-\Delta/T_c}$, respectively.

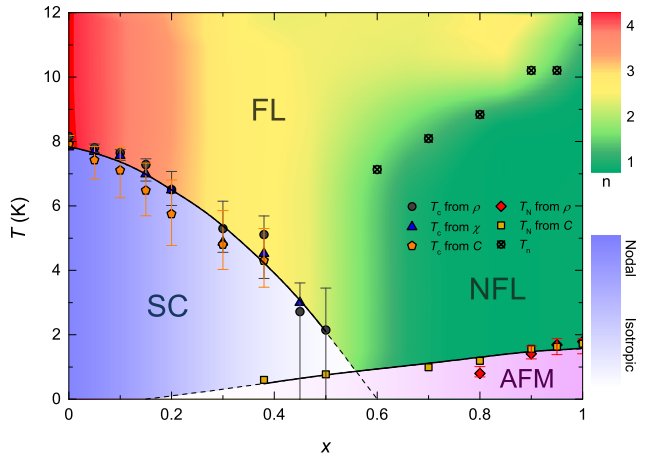

FIG. 8: (Color online) A plot of temperature T versus Eu concentration x, $(T - x)$, phase diagram. The vertical bars in the $T_c(x)$ data represent the widths of the superconducting transitions (see text). The suppression of T_c with x has negative curvature and extrapolates to 0 K near $x = 0.6$. The blue gradient-filled area under the T_c versus x curve represents the change of the temperature-dependence of low-temperature specific heat, $C_e/\gamma T_c = b(T_c/T)^{-m}$ to $ae^{-\Delta/T_c}$. The Néel temperature T_N decreases slowly from $x = 1$ to $x \simeq 0.38$. SC and AFM may coexist in the region between $x \simeq 0.2$ and $\simeq 0.6$. The black circles with crosses are the temperatures, T_n, where resistivity slopes have kinks as seen in Fig. 3(a). The color contour plot in the background displays the evolution of the power n values in the formula, $\log(\rho(T) - \rho_0) = \log(A_n) + n\log(T)$.

compounds [5]. In the case of nodes in the gap structure, it is intriguing to note that such a change in m values from ~ 3 to ~ 2 may suggest that the gap structure evolves from point-like to line nodes [33]. In Fig. 7 (d,e,f), the blue lines are the fits of an exponential temperature dependence, $ae^{-\Delta/T_c}$, where a is a fitting parameter and Δ is the SC energy gap; these values are listed in Fig. 7 (d,e,f). These results suggest that the compounds with $x \geq 0.15$ exhibit single-band isotropic s-wave SC.

Similar crossovers or changes from power law to exponential temperature dependence in $C(T)$ the superconducting state were observed in previous studies for the $Pr(Os_{1-x}Ru_x)_4Sb_{12}$, $Pr_{1-x}Ce_xPt_4Ge_{12}$, $La_{1-x}Ce_xPt_4Ge_{12}$, and $PrPt_4Ge_{12-x}Sb_x$ systems [12, 13,34,35]. A possible explanation for this change is a crossover in the superconducting energy gap from point-nodes to nodeless structures, or a suppression of one or more superconducting energy gaps in a multiband superconductor [5,10,11,33]. Recently, low-temperature specific heat measurements on $Pr_{1-x}Ce_xPt_4Ge_{12}$ suggest the presence of both a nodal and a nodeless gap on different parts of the Fermi surface in $PrPt_4Ge_{12}$, which are suppressed with different rates upon increasing Ce substitutions [14]. This scenario would be another explanation for the non-integer values of m in the $x = 0.05$ and 0.1 data and the low-temperature upturns or deviations from the linear fits for the $x = 0.15$ and 0.2 samples. However, the latter deviations could also be due to the fact that the values of Δ/T_c could vary depending on the fitting range [36]. More detailed studies of low-temperature specific heat on the $Pr_{1-x}Eu_xPt_4Ge_{12}$ system are underway. These studies will be able to discriminate between these different scenarios and will reveal the nature of the superconducting order parameters and their evolution with Eu concentration.

IV. DISCUSSION

Figure 8 summarizes the results from $\rho(T)$, $\chi(T)$, and $C(T)$ measurements in a temperature, T, versus europium, x, $(T - x)$, phase diagram. The SC transition temperature, T_c, values were taken from the onset of diamagnetic signals in the $\chi(T)$ data. For the $C(T)$ measurements, T_c was determined from the results of idealized entropy-conserving constructions [37,38] (data not shown). The error bars were taken from the width of transitions in both resistivity and specific heat data. These T_c values estimated by different measurements exhibit a consistent trend, in which SC is suppressed with negative curvature up to $x \simeq 0.6$. The suppression rate of T_c for $Pr_{1-x}Eu_xPt_4Ge_{12}$ is different compared to our previous substitution studies of $Pr_{1-x}Ce_xPt_4Ge_{12}$ and

$PrPt_4Ge_{12-x}Sb_x$, which show suppressions of T_c with positive curvature [12,13]. Since Eu ions have a stable divalent electronic state in the skutterudite structure [24], the crystalline electric field effects are expected to be absent. Thus, we could consider the effect on SC of substituting Eu^{+2} ions as similar to that of substituting Gd^{3+} for Pr. The monotonic change of our $\mu_{\rm eff}$ data (see Fig. 4(c)) supports this scenario. Rare earth impurities with stable valences are believed to exhibit ferromagnetic exchange interactions with a host superconductor (this case, $PrPt_4Ge_{12}$) wherein the depression of T_c with paramagnetic impurity concentration is described by the Abrikosov-Gor'kov (AG) theory [39], as has been demonstrated for the $La_{1-x}Gd_xAl_2$ system [40]. The negative curvature of $T_c(x)$ in this study seems to be consistent with the AG theory, compared to the results of the Ce substitution study, in which the depression of T_c with x resembles the behavior expected for a system in which the paramagnetic impurities produce a Kondo effect in which the Kondo temperature is much larger than the SC transition temperature T_c. On the other hand, the substitution of Eu^{2+} ions (hole doping), is different from that of Gd^{3+} (isoelectronic substitution). The doping into the Pr site may have a weaker effect on SC than doping into the Pt-Ge cage, since the Fermi surface of $PrPt_4Ge_{12}$ is mainly composed of the Ge-4*p* orbitals with small contributions from the Pt-5*d* orbitals [7]. In the SC states of the $Pr_{1-x}Eu_xPt_4Ge_{12}$ system, the situation is more complicated than in $La_{1-x}Gd_xAl_2$, as we observed evidence for a crossover in the SC energy gap from point-nodes to nodeless structures, or a suppression of one or more superconducting energy gaps in a multiband superconductor [5,10,11,14,33]. This crossover behavior is depicted by color gradient below the T_c versus x curve in Fig. 8.

The Néel temperatures, T_N, were consistent between the $\rho(T)$ and the low-temperature $C(T)$ data. The $Pr_{1-x}Eu_xPt_4Ge_{12}$ system exhibits a crossover from SC to AFM states with increasing x and, more interestingly, a coexistence of those two states in the range of $0.2 \simeq x \simeq 0.6$. Such a coexistence of AFM and SC has been observed in other conventional and unconventional SC containing localized magnetic moments [41–43]. As recently suggested by Singh *et al.* [14], our system seems to show that the nodal gap is being suppressed relatively slowly upon Eu substitution in the SC and coexistence regions, compared to the rapid suppressions observed in previous reports [12,13]. In the non-ordered states, i.e., the high-temperature region, the system shows an evolution of the power dependence of the resistivity in the formula $\rho(T) = \rho_0 + AT^n$, shown as a color contour plot in Fig. 8. The values of n change from $n \sim 5$ at Pr rich sites to $n \sim 2$ (FL behavior) at $x \sim 0.5$, and then enters a NFL state with $n \sim 1$ at Eu rich sites. Such FL to NFL transition is also manifested by small kinks observed in the resistivity data (see Fig. 3). In the specific heat data, we did not observe a very clear logarithmic divergence (data not shown), $C(T)/T \sim (-1/T_0)\ln(T/T_0)$, which is believed to be a nearly universal feature of NFL behavior in specific heat [44]; however, a weak power-law divergence could be also an indication for NFL behavior [44] and the divergence in specific heat could vary between different systems [45]. Therefore, we speculate that the rather large jumps in the specific heat for the Eu rich compounds are possibly the combination of AFM transitions and the divergence due to the NFL behavior. However, there are other possible scenarios for the observed kinks in resistivity, for example, subtle structural phase transitions, which have been reported in skutterudite-related systems [46].

Our study of $Pr_{1-x}Eu_xPt_4Ge_{12}$ shows a complex phase diagram with SC to AFM and FL to NFL crossovers, suggesting that changes in the underlying electronic structure "tune" competing interactions in this system; this interpretation could be supported by the scenario of multiband type of SC with different energy gap structures in $PrPr_4Pt_{12}$ [9–11,14]. Since there is no report of the $GdPt_4Ge_{12}$ compound, it would be interesting to perform a substitution study of $Pr_{1-x}Gd_xPt_4Ge_{12}$ as a comparative study with the current study. Subsequent studies of density functional theory (DFT) calculations on $Pr_{1-x}(Eu,Gd)_xPt_4Ge_{12}$ would give us better understanding of the relationship of the electronic density of states (DOS) and paramagnetic impurities on the nature of unconventional SC in $PrPt_4Ge_{12}$.

V. CONCLUDING REMARKS

We studied the superconducting and normal-state properties of the unconventional superconductor $PrPt_4Ge_{12}$, in which Eu has been substituted for Pr. Polycrystalline samples of $Pr_{1-x}Eu_xPt_4Ge_{12}$ were investigated via x-ray diffraction, electrical resistivity, magnetic susceptibility, and specific heat measurements. Upon Eu substitution, we observed a crossover from superconducting to antiferromagnetically ordered states with a region where superconductivity and antiferromagnetism may coexist. In the superconducting region, the specific heat data exhibit a crossover of temperature dependence, suggesting a change from a nodal to a nodeless superconducting energy gap or suppression of multiband superconductivity. This crossover is relatively slower than previous reports of different substitution studies, suggesting paramagnetic impurities have weaker pair breaking effect on the unconventional superconductivity in $PrPt_4Ge_{12}$. In the normal state, we observed a crossover from Fermi-liquid to non-Fermi-liquid behavior, accompanied by a coexistence of superconductivity and antiferromagnetism, suggesting intrinsic electronic structures may be correlated with the complex physical phenomena in this system.

Acknowledgments

This work was supported by the U. S. Department of Energy, Office of Basic Energy Sciences, Division of Materials Sciences and Engineering under Grant No. DE-FG02-04-ER46105 (characterization and physical properties measurements), and the National Science Foundation under Grant No. DMR 1206553 and DMR 1506677 (low-temperature resistivity measurements). The work at KSU was supported by the National Science Foundation under Grant No. DMR 1505826 (low-temperature specific heat measurements).

* Corresponding Author: mbmaple@ucsd.edu

[1] E. Bauer, A. Grytsiv, X.-Q. Chen, N. Melnychenko-Koblyuk, G. Hilscher, H. Kaldarar, H. Michor, E. Royanian, G. Giester, M. Rotter, et al., Phys. Rev. Lett. **99**, 217001 (2007).
[2] E. Bauer, X.-Q. Chen, P. Rogl, G. Hilscher, H. Michor, E. Royanian, R. Podloucky, G. Giester, O. Sologub, and A. P. Gonçalves, Phys. Rev. B **78**, 064516 (2008).
[3] R. Gumeniuk, W. Schnelle, H. Rosner, M. Nicklas, A. Leithe-Jasper, and Y. Grin, Phys. Rev. Lett. **100**, 017002 (2008).
[4] M. Toda, H. Sugawara, K. ichi Magishi, T. Saito, K. Koyama, Y. Aoki, and H. Sato, J. Phys. Soc. Jpn. **77**, 124702 (2008).
[5] A. Maisuradze, M. Nicklas, R. Gumeniuk, C. Baines, W. Schnelle, H. Rosner, A. Leithe-Jasper, Y. Grin, and R. Khasanov, Phys. Rev. Lett. **103**, 147002 (2009).
[6] F. Kanetake, H. Mukuda, Y. Kitaoka, H. Sugawara, K. Magishi, K. M. Itoh, and E. E. Haller, Physica C **470**, S703 (2010).
[7] R. Gumeniuk, H. Borrmann, A. Ormeci, H. Rosner, W. Schnelle, M. Nicklas, Y. Grin, and A. Leithe-Jasper, Z. Kristallogr. **225**, 531 (2010).
[8] A. Maisuradze, W. Schnelle, R. Khasanov, R. Gumeniuk, M. Nicklas, H. Rosner, A. Leithe-Jasper, Y. Grin, A. Amato, and P. Thalmeier, Phys. Rev. B **82**, 024524 (2010).
[9] L. S. S. Chandra, M. K. Chattopadhyay, and S. B. Roy, Phil. Mag. **92**, 3866 (2012).
[10] Y. Nakamura, H. Okazaki, R. Yoshida, T. Wakita, H. Takeya, K. Hirata, M. Hirai, Y. Muraoka, and T. Yokoya, Phys. Rev. B **86**, 014521 (2012).
[11] J. L. Zhang, Y. Chen, L. Jiao, R. Gumeniuk, M. Nicklas, Y. H. Chen, L. Yang, B. H. Fu, W. Schnelle, H. Rosner, et al., Phys. Rev. B **87**, 064502 (2013).
[12] K. Huang, L. Shu, I. K. Lum, B. D. White, M. Janoschek, D. Yazici, J. J. Hamlin, D. A. Zocco, P.-C. Ho, R. E. Baumbach, et al., Phys. Rev. B **89**, 035145 (2014).
[13] I. Jeon, K. Huang, D. Yazici, N. Kanchanavatee, B. D. White, P.-C. Ho, S. Jang, N. Pouse, and M. B. Maple, Phys. Rev. B **93**, 104507 (2016).
[14] Y. P. Singh, R. B. Adhikari, S. Zhang, K. Huang, D. Yazici, I. Jeon, M. B. Maple, M. Dzero, and C. C. Almasan, Phys. Rev. B **94**, 144502 (2016).
[15] D. C. Johnston, Advances in Physics **59**, 803 (2010).
[16] G. R. Stewart, Rev. Mod. Phys. **83**, 1589 (2011).
[17] P.-C. Ho, T. Yanagisawa, W. M. Yuhasz, A. A. Dooraghi, C. C. Robinson, N. P. Butch, R. E. Baumbach, and M. B. Maple, Phys. Rev. B **83**, 024511 (2011).
[18] D. E. MacLaughlin, P.-C. Ho, L. Shu, O. O. Bernal, S. Zhao, A. A. Dooraghi, T. Yanagisawa, M. B. Maple, and R. H. Fukuda, Phys. Rev. B **89**, 144419 (2014).
[19] A. Grytsiv, X.-Q. Chen, N. Melnychenko-Koblyuk, P. Rogl, E. Bauer, G. Hilscher, H. Kaldarar, H. Michor, E. Royanian, R. Podloucky, et al., J. Phys. Soc. Jap. **77**, 121 (2008).
[20] E. D. Bauer, A. Slebarski, N. A. Frederick, W. M. Yuhasz, M. B. Maple, D. Cao, F. Bridges, G. Giester, and P. Rogl, J. Phys.: Condens. Matter **16**, 5095 (2004).
[21] C. Sekine, K. Akahira, K. Ito, and T. Yagi, J. Phys. Soc. Jpn. **78**, 093707 (2009).
[22] V. V. Krishnamurthy, J. C. Lang, D. Haskel, D. J. Keavney, G. Srajer, J. L. Robertson, B. C. Sales, D. G. Mandrus, D. J. Singh, and D. I. Bilc, Phys. Rev. Lett. **98**, 126403 (2007).
[23] C. Sekine, M. Inoue, T. Inaba, and I. Shirotani, Physica B: Condensed Matter **281282**, 308 (2000).
[24] M. Nicklas, R. Gumeniuk, W. Schnelle, H. Rosner, A. Leithe-Jasper, F. Steglich, and Y. Grin, J. Phys.: Conf. Ser. **273**, 012118 (2011).
[25] A. C. Larson and R. B. V. Dreele, Los Alamos National Laboratory Report, 1994 (unpublished).
[26] B. Toby, J. Appl. Crystallogr. **34**, 210 (2001).
[27] B. D. White, K. Huang, and M. B. Maple, Phys. Rev. B **90**, 235104 (2014).
[28] R. M. Galra, C. Opagiste, M. Amara, M. Zbiri, and S. Rols, J. of Phys.: Conf. Ser. **592**, 012011 (2015).
[29] N. F. Mott and H. Jones, *The theory of the properties of metals and alloys* (Dover Publications Inc., New York, 1958).
[30] M. Nicklas, S. Kirchner, R. Borth, R. Gumeniuk, W. Schnelle, H. Rosner, H. Borrmann, A. Leithe-Jasper, Y. Grin, and F. Steglich, Phys. Rev. Lett. **109**, 236405 (2012).
[31] E. D. Bauer, N. A. Frederick, P.-C. Ho, V. S. Zapf, and M. B. Maple, Phys. Rev. B **65**, 100506 (2002).
[32] M. B. Maple, P.-C. Ho, V. S. Zapf, N. A. Frederick, E. D. Bauer, W. M. Yuhasz, F. M. Woodward, and J. W. Lynn, J. Phys. Soc. Jpn. **71**, 23 (2002).
[33] M. Sigrist and K. Ueda, Rev. Mod. Phys. **63**, 239 (1991).
[34] N. A. Frederick, T. A. Sayles, S. K. Kim, and M. B. Maple, J. Low Temp. Phys. **147**, 321 (2007).
[35] K. Huang, D. Yazici, B. D. White, I. Jeon, A. J. Breindel, N. Pouse, and M. B. Maple, Phys. Rev. B **94**, 094501 (2016).
[36] G. Gladstone, M. A. Jensen, and J. R. Schrieffer, in *Superconductivity*, edited by R. D. Parks (Marcel Dekker, New York, 1969), vol. 2, p. 699.
[37] E. Bonjour, R. Calemczuk, J. Y. Henry, and A. F. Khoder, Phys. Rev. B **43**, 106 (1991).
[38] S. B. Ota, V. S. Sastry, E. Gmelin, P. Murugaraj, and J. Maier, Phys. Rev. B **43**, 6147 (1991).
[39] A. A. Arikosov and L. P. Gor'kov, Sov. Phys.-JETP **12**, 1243 (1961).
[40] M. B. Maple, E. D. Bauer, V. S. Zapf, and J. Wosnitza, in *Superconductivity, Conventional and Unconventional Superconductors*, edited by K. H. Bennemann and J. B. Ket-

terson (Springer, Berlin, 2008), vol. 1, p. 693.
[41] R. McCallum, D. Johnston, R. Shelton, and M. Maple, Solid State Commun. **24**, 391 (1977).
[42] M. Ishikawa and . Fischer, Solid State Commun. **24**, 747 (1977).
[43] X. F. Lu, N. Z. Wang, H. Wu, Y. P. Wu, D. Zhao, X. Z. Zeng, X. G. Luo, T. Wu, W. Bao, G. H. Zhang, et al., Nat. Mater. **14**, 325 (2015).
[44] M. B. Maple, R. E. Baumbach, N. P. Butch, J. J. Hamlin, and M. Janoschek, J. Low Temp. Phys. **161** (2010).
[45] L. Zhu, M. Garst, A. Rosch, and Q. Si, Phys. Rev. Lett. **91**, 066404 (2003).
[46] A. Ślebarski, M. Fijałkowski, M. M. Maśka, M. Mierzejewski, B. D. White, and M. B. Maple, Phys. Rev. B **89**, 125111 (2014).